WEP Warwick Evans Publishing

International Journal of Natural Resources and Environmental Studies

ISSN: 3006-2012 (Print), ISSN: 3006-0834 (Online) | Volume 7, Number 3, Year 2025
DOI: https://doi.org/10.62051/ijnres.v7n3.03
Journal homepage: https://wepub.org/index.php/IJNRES/index

Monitoring and Analysis of Spatiotemporal Variations in Poyang Lake (2016–2024) Using Sentinel-1/2 Imagery

Yuhao Sun and Hailiang Jin*

School of Surveying and Land Information Engineering, Henan Polytechnic University, Jiaozuo 454003, China

*Corresponding Author: Hailiang Jin

ABSTRACT

Timely and accurate information on dynamic open surface water is essential for under-standing long-term hydrological patterns and sustainable development. Frequent cloud cover limits the use of optical imagery for dynamic surface water observation, making it difficult to achieve high-frequency monitoring. A high-frequency surface water observa-tion dataset for Poyang Lake from 2016 to 2024 was constructed by employing a rapid ex-traction algorithm that integrates Sentinel-1/2 imagery. Subsequently, the spatiotemporal changes of the lake's surface water over the 2016–2024 period. Our findings indicate that the extraction algorithm achieved a high degree of accuracy, with Overall Accuracies (OA) exceeding 95% and Kappa coefficients greater than 0.90. The dataset reveals a significant seasonal trend, with the maximum inundation area occurring in 2020 (5,179 km²) and the minimum in 2022 (3,196.04 km²). The water area typically peaks in June–July and recedes to its minimum in November–December. Permanent and temporary water bodies are de-creasing, while seasonal ones are increasing. The conversion between water body types was dominated by the reclassification of temporary and permanent water as seasonal water. These research findings provide key data on the recent hydrological dynamics of Poyang Lake.

KEYWORDS

Water body extraction, Sentinel, Edge Otsu, Poyang Lake, Spatiotemporal variation.

1. INTRODUCTION

Water on the Earth's surface, which are extensively distributed across the terrestrial surface, primarily comprise oceans, rivers, lakes, reservoirs, wetlands, and swamps [1]. As the most crucial water resource reserves in the terrestrial environment, they provide the bedrock for human existence. Moreover, the contribution of surface water systems to climate change, the hydrological cycle, and the maintenance of ecological stability is vital, and they also provide vital resources for diverse life forms [2,3]. The variations in surface water are also inherently connected to social and economic factors, supporting numerous human endeavors and economic growth by providing services such as drinking water, agricultural irrigation and aquaculture [4,5]. As the world's population surges and economies expand swiftly, the demand for water is constantly rising, making the contradiction between supply and demand progressively prominent [6]. In China, this issue is exacerbated by the uneven distribution of water resources between the north and south. Consequently, the challenge of water resources has become one of the primary constraints hindering the nation's economic development and ecological environmental protection. Furthermore, the morphology of surface water can be swiftly modified by episodes of extreme rainfall and drought, which often culminate in hydrological disasters [7]. For conducting water resource surveys, elevating water resource management standards, monitoring and assessing hydrological calamities, and facilitating sustainable

socioeconomic development, understanding the dynamic shifts in water resources possesses considerable practical importance.

The advancement of remote sensing technology has been swift, establishing it as a highly efficient tool for gathering surface water data. Unlike conventional field surveys, this technology offers distinct benefits such as extensive geographical reach, quick data refresh, frequent observation capabilities, and comprehensive spectral insights [8]. Numerous satellite systems can now be utilized for extracting surface water information, including MODIS [9], Landsat [10], and Sentinel [11]. To accommodate the diversity of data sources and their distinct characteristics, researchers have proposed various water body extraction methods, a major group of which includes threshold-based segmentation techniques [12] and machine learning algorithms [13]. Considering the variability of water's spectral properties across space and time, the combination of multiple indices can achieve better extraction results than a single index [14]. Zou et al. [15] tracked the dynamics of U.S. surface water over many years, utilizing a combination of three water indices. Xing et al. [16] investigated the multi-year spatiotemporal dynamics of lakes across the Inner Mongolia Plateau. Deng et al. [17] proposed the Multi-band Water Detection Rule (MIWDR). Through comparison, it was found that the new extraction rule performs better in urban environments. Based on the new extraction rule, Xing et al. [18] investigated the evolution of water surface area in Shandong Province over three decades, and a similar assessment was performed by Wang et al. [19] for Dongting Lake.

In previous studies, large-scale monitoring of annual dynamic changes has predominantly relied on the Landsat series of satellites. However, the long revisit period of Landsat makes it vulnerable to cloud cover and rainfall. Moreover, water bodies exhibit significant seasonal and interannual variability, particularly in regions with pronounced monsoon climates, which complicates high-frequency monitoring. The Sentinel-2 high-resolution multispectral satellite, with a revisit period of 6 days, presents significant potential for high-frequency monitoring and dynamic analysis of water bodies. Conse-quently, numerous studies have now utilized Sentinel-2 imagery for water body monitoring [20].

With limited band information, water bodies are typically identified based on the differences in backscattering coefficients among various surface features. The primary methods for this discrimination include single-threshold and OTSU automatic threshold segmentation. Using Sentinel-1 as the data source, Zeng et al. [21] extracted Poyang Lake's water bodies utilizing Otsu's method. Moreover, the conventional Otsu's method, an automatic thresholding algorithm based on image histograms, exhibits significant performance degradation when the target feature is significantly smaller than the background. In such cases, the Edge Otsu method, which can also automatically compute a threshold, has been shown to outperform the traditional Otsu method in similar scenarios [22]. The impact of different initial threshold settings on the Edge Otsu algorithm's results were also analyzed by Wang et al [23]. For large-scale remote sensing monitoring tasks, it is often challenging to achieve high-frequency data acquisition and clear image details simultaneously. The combination of optical and radar data can effectively address this challenge [24]. However, the collaborative analysis of diverse datasets places high demands on data acquisition and computational power. The Google Earth Engine (GEE) possesses extensive datasets and robust computational and storage capabilities, can effectively address this challenge.

Poyang Lake serves vital functions in flood control, irrigation, water supply, and maintaining biodiversity. Concurrently, the lake's water body exhibits significant seasonal variations, which underscores the particular importance of high-frequency dynamic monitoring of the lake. The primary purpose of this study is to: (1) To enable a multi-year, dynamic monitoring framework for Poyang Lake using Sentinel series imagery. (2) To examine spatiotemporal characteristics of Poyang Lake’s surface extent and inundation frequency during 2016–2024, including the dynamics of and conversions between different water body types. (3) To examine the potential natural and human-induced drivers responsible for fluctuations in water area.

2. MATERIALS AND METHODS

2.1. Study Area

Functioning as a significant lake subsystem in the downstream portion of the Yangtze River's hydrological system, Poyang Lake is situated in northern Jiangxi Province (Figure 1). Influenced by a monsoon climate, precipitation in the region is highly seasonal, with approximately 70% concentrated in the wet season, and exhibits significant inter-annual variability and uneven intra-annual distribution. Consequently, Poyang Lake undergoes substantial changes in its water coverage with the seasons, expanding to over 4,000 km² in the high-water period and shrinking to less than 1,000 km² in the low-water period, a process that exposes vast expanses of mudflats. This combination of complex topography and climatic conditions makes Poyang Lake a region highly prone to flood events.

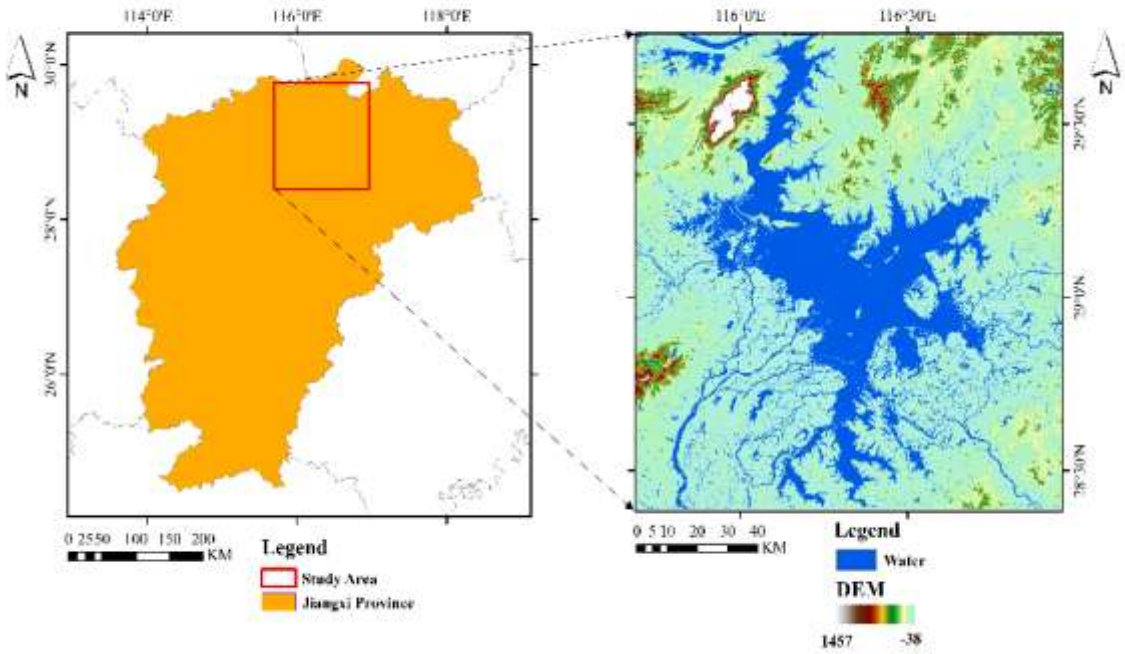

Figure 1: Poyang Lake's location in Jiangxi Province and its geographical location.

2.2. Data and processing

2.2.1. Sentinel-1/2 datasets

Across 13 spectral bands, the sensor on Sentinel-2 gathers data. Its dual-satellite constellation ensures a 5-day revisit period. Sentinel-2 data are disseminated as Level-1C and Level-2A products. In this research, Level-1C data were utilized for the extraction of the maximum inundation extent. Initially, we filtered the image collection to select scenes with a 'CLOUDY_PIXEL_PERCENTAGE' of less than 20%. After comparing different cloud masking algorithms, we found that the most effective approach was to use the Cloud Score+ algorithm available on GEE. Opaque and cirrus clouds were removed using the Quality Assessment (QA) band from Cloud Score+. Subsequently, atmospheric correction was performed on the cloud-masked Sentinel-2 imagery using the Py6s model. Finally, the images underwent further preprocessing, including mosaicking and clipping to the study area, for the final water body extraction.

The Sentinel-1 constellation consists of two satellites that provide a combined revisit period of 6 days when both satellites are operational, with an onboard sensor capable of operating in four operational modes. For this research, we utilized imagery from the Interferometric Wide swath (IW) mode, which had already undergone pre-processing. Subsequently, these data were terrain-corrected, and the Perona-Malik algorithm was applied for filtering to smooth the image and suppress speckle noise while preserving edge information. Finally, images from the same orbital direction (ascending and descending) were mosaicked.

2.2.2. Other ancillary data

Database for Hydrological Time Series of Inland Waters (DAHITI) is a dataset designed for storing, sharing, and analyzing long-term hydrological time series data from inland water bodies (such as reservoirs, lakes, and river segments) [25]. We acquired water level data for the study area from 2016 to 2024 from DAHITI to verify the reliability of our experimental results.

The ERA5 reanalysis product was the source for monthly precipitation and evaporation data covering the study area from 2016 to 2024. (available at: https://www.ecmwf.int/, last accessed on 1 June 2025).

The JRC Monthly Water History [4] documents the monthly extent of surface water, derived from Landsat satellite data, which is used to track and analyze fluctuations in surface water coverage since 1984. The Global Surface Water Dynamics dataset [26] characterizes the dynamic changes and inter-annual features of global inland water extent through multiple indicators. In this study, both datasets were primarily used for a comparative analysis against our extraction results.

We utilized the NASA Digital Elevation Model for the terrain correction of Sentinel-1 imagery and to calculate slope, which allowed for the exclusion of areas with slopes greater than 20° to reduce interference from terrain shadows [27]. Surface water has a natural tendency to collect in topographical lows within a drainage basin, Height Above Nearest Drainage (HAND) data [28] were also utilized to effectively exclude regions where surface water occurrence is topographically implausible.

2.3. Method

Figure 2 illustrates the workflow for the lake surface analysis. First, a map of the maximum inundation extent from 2016–2024 was generated from processed Sentinel-2 time-series imagery by combining multiple water indices and calculating water frequency. Subsequently, the Edge Otsu algorithm was applied for feature extraction on the preprocessed Sentinel-1 imagery, which were then post-processed to exclude areas where surface water occurrence is topographically implausible. Finally, the definitive lake surface extraction was achieved by intersecting the Sentinel-2-derived maximum inundation extent with the results obtained from Sentinel-1. Based on these final results, the analysis focused on how the lake's area has changed over time and space, along with an investigation into the potential drivers behind these trends.

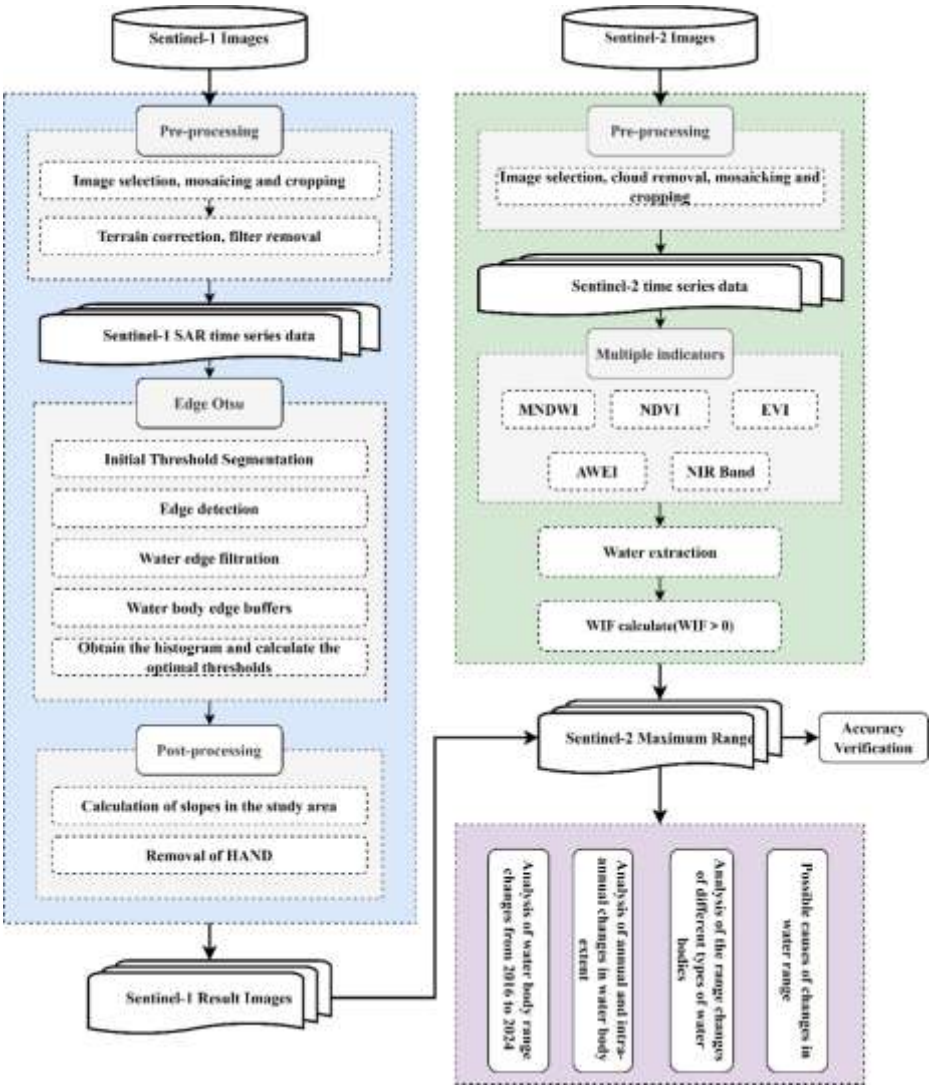

Figure 2: Technical flow chart of this article.

2.3.1. Multi-index water body detection rules based on optical images

The water extraction algorithm proposed by Liu et al. [29], which integrates multiple water indices, has been proven to offer significant advantages in extraction accuracy. This method primarily combines the Modified Normalized Difference Water Index (MNDWI) [30], the Automated Water Extraction Index (AWEI) [31], the Normalized Difference Vegetation Index (NDVI) [32], and the Enhanced Vegetation Index (EVI) [33]. Additionally, to exclude high-reflectance features, we utilize the Near-Infrared (NIR) band value. In our study, we apply Equations (1)-(7) for water extraction. A pixel is classified as water and assigned a value of 1 if the condition specified in Equation (7) is satisfied.

$$\mathrm{NIR} < 0.17. \tag{1}$$

$$MNDWI = \frac{Green\ -\ SWIR1}{Green\ +\ SWIR1}. \tag{2}$$

$$EVI = 2.5 \times \frac{NIR - Red}{NIR\ +6\times\ Red\ -7.5\times\ Blue\ +1}. \tag{3}$$

$$NDVI = \frac{NIR - Red}{NIR + Red}. \tag{4}$$

$$AWEI_{nsh} = 4 \times (Green - SWIR1) - (0.25 \times NIR + 2.75 \times SWIR2). \tag{5}$$

$$AWEI_{sh} = Blue + 2.5 \times Green - 1.5 \times (NIR + SWIR1) - 0.25 \times SWIR2 . \quad (6)$$

$$\begin{cases} (MNDWI > EVI) \text{ or } (mNDWI > NDVI)] \text{ and } NIR < 0.17 \\ \text{and } \left(AWEI_{nsh} > -0.88 or\ AWEI_{sh} > -0.27\right) \text{and } \left(AWEI_{nsh} - AWEI_{sh}\right) > -0.2 \end{cases} . \quad (7)$$

Where NIR, Green, Red, Blue, SWIR1, SWIR2, are the B8, B3, B4, B2, B11 and B12 bands of Sentinel-2, respectively.

2.3.2. Edge Otsu

The Edge Otsu algorithm calculates an optimal threshold for each individual image, effectively overcoming the limitations of the conventional Otsu method. The process begins with an initial binary classification of the image using a preliminary threshold. Next, we employ the Canny edge detector to identify the perimeters of water bodies. Subsequently, the detected edges undergo processing to remove weaker edges, resulting in clearer and cleaner boundaries while mitigating noise interference. By calculating the number of connected pixels around each pixel, isolated or poorly connected edges are eliminated, ensuring that the retained edges are both prominent and coherent. Finally, the Otsu algorithm is applied to the histogram generated from sampling pixels within the edge buffer zone, which yields the final image-wide segmentation threshold. (Figure 3).

The initial segmentation threshold has a significant impact on the results of binary classification. Regarding the selection of the buffer parameter, the quality of the histogram is dependent on the chosen buffer size; an improperly sized buffer, whether too large or too small, can negatively affect the quality of the water extraction. Therefore, based on this literature [23][34], an initial -17.5 dB threshold and a 500 m buffer were utilized in this study.

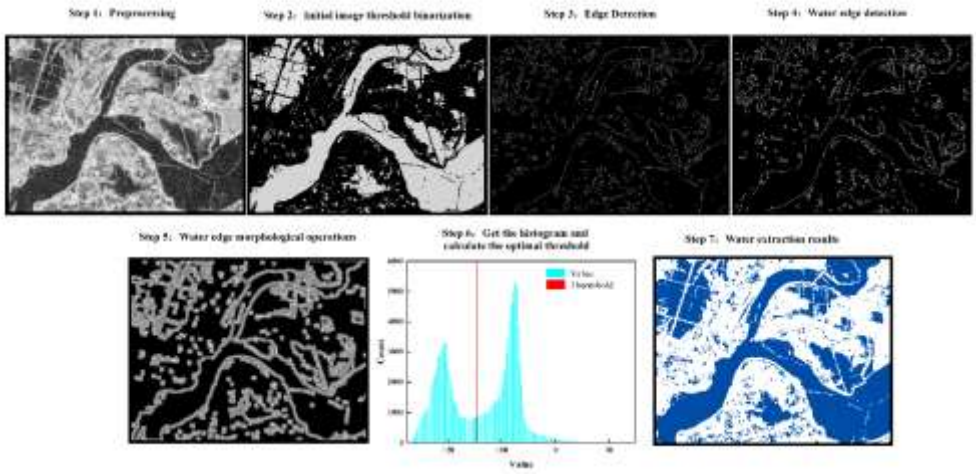

Figure 3: Edge Otsu algorithm flow: preprocessing, initial image binarization, edge detection, water body edge detection, water body edge morphological operation, obtain histogram and calculate the optimal threshold, water body extraction results.

2.3.3. Accuracy assessment

Poyang Lake exhibits significant seasonal differences. Therefore, a validation date was randomly selected for both the periods of high rainfall and low rainfall. Utilizing Sentinel-2 imagery as the primary reference, supplemented by Sentinel-1 imagery, we randomly generated 1600 sample points throughout the area of interest for visual interpretation. Based on the resulting confusion matrix, we calculated several evaluation metrics.

Furthermore, the differences between the extraction results and other datasets were quantified utilizing relative error. This was computed as shown in Equation (8):

$$E_r(\%) = \frac{|x - x_t|}{|x_t|} \times 100\%. \quad (8)$$

Where, E_r represents the relative percentage error, x is the result of other datasets, and x_t is the extraction result of this article.

2.3.4. Calculation of water inundation frequency

The formula for calculating water frequency is as follows:

$$F_p = \frac{\sum_{i=1}^{N} w}{N_{\text{total}}} \times 100\%. \quad (9)$$

Where N_{total} denotes the total number of valid observations over the entire observation period from 2016 to 2024, and w has two possible states (1 if identified as water, 0 if identified as non-water). If a pixel has an F_p-value of 75% or greater, it is considered permanent water. If a pixel has a water frequency F_p-value 25% or less, it is considered as temporary water. The remaining pixels are considered seasonal water bodies.

2.3.5. Trend testing and correlation analysis

To analyze temporal trends in water bodies across various seasons and types, the Mann-Kendall (MK) trend test was applied. The correlation between water Inundation extent and other variables was examined using Pearson correlation analysis.

3. RESULTS

3.1. Accuracy evaluation

Sentinel-1 images from periods of high rainfall (July 26, 2019) and periods of low rainfall (November 12, 2021) were randomly selected for accuracy validation, in conjunction with Sentinel-2 imagery from adjacent dates. Overall accuracies of 0.989 and 0.964 were achieved for water identification during high and low rainfall periods, respectively. The corresponding Kappa coefficients were 0.978 and 0.918 (Table 1). The Edge Otsu algorithm has demonstrated its high suitability for water body extraction in the Poyang Lake region, thereby permitting batch extraction across different time series.

Table 1: Confusion matrix for the extraction results

	Samples	Visual interpretation		Total	User Accuracy
		Water	Non-water		
July 2019	Water	798	15	813	99.75%
Sentinel1/2	Non-water	2	785	787	98.12%
	Total	800	800	1600	Overall accuracy=98.94%
	Producer accuracy	98.15%	99.74%		Kappa=97.87%
November 2021	Water	490	46	536	97.80%
Sentinel1/2	Non-water	11	1053	1064	95.81%
	Total	501	1099	1600	Overall accuracy=96.43%
	Producer accuracy	91.41%	98.96%		Kappa=91.87%

3.2. Analysis of fluctuations in Water extent

Poyang Lake's water area exhibits significant seasonal fluctuations and inter-annual differences (Figure 4), which fully reflects its typical characteristics as a seasonal, river-fed fluctuating lake. Throughout the observation period, the average inundation area was 3196.04 km². Analysis of the Inundation extent revealed that the maximum extent occurred on July 20, 2020, reaching an area of 5179.37km². Conversely, the minimum water area was observed on November 19, 2022, measuring 1656.83 km² (Figure 5). Analysis of the 2016–2024 time series revealed a statistically non-significant upward trend in the water surface area (Z = 0.2375, p > 0.05).

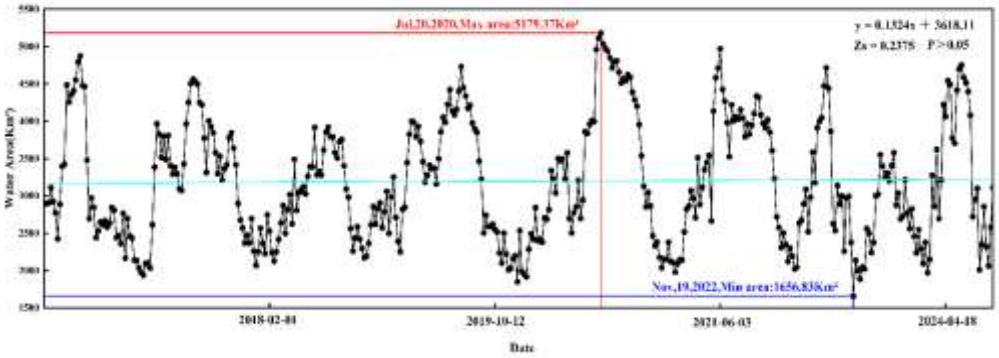

Figure 4: Time series of water extent (2016–2024).

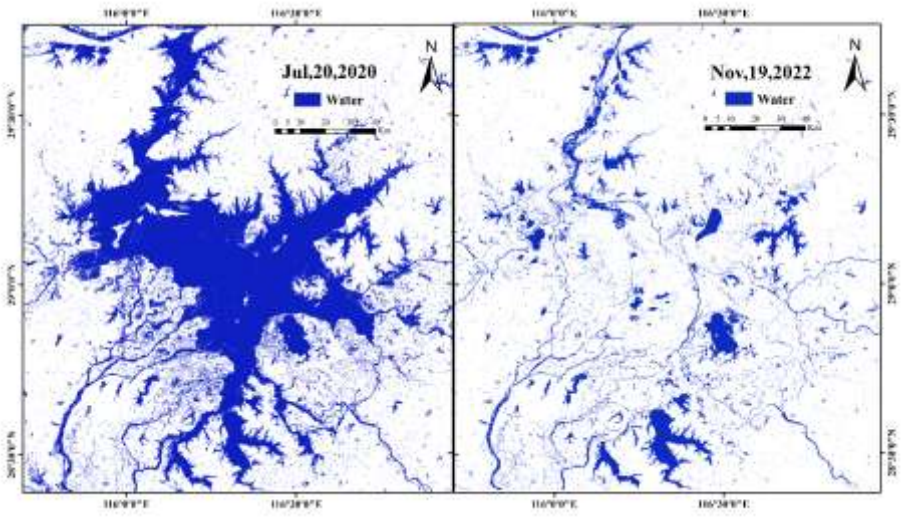

Figure 5: Maximum and minimum water inundation extent (2016–2024).

3.3. Analysis of Monthly Changes

According to the statistical analysis results (Figure 6), the lake's water area demonstrates pronounced intra-annual variations. The maximum monthly average water area was observed in July at 4220.85 km², whereas the minimum monthly average occurred in December, measuring 2382.60 km².Further analysis of the extreme values shows that the absolute maximum for a monthly water area was 5179.37 km², recorded in July 2020, while the smallest of the monthly maximums was 3110.16 km² in December 2024. Regarding the monthly minimums, the highest value recorded was 2943.97 km² in June 2020, and the lowest value was 1656.83 km² in November 2022. Consequently, these findings indicate that June and July are typically the months of maximum water extent, while November and December are the months of minimum water extent.

We classified the annual hydrological cycle into two distinct periods. The wet season, comprising the months from April to October, was characterized by a significant expansion of the water surface area, with a monthly maximum consistently exceeding 4,000 km², a minimum area always above 2,000 km², and an average of over 3,000 km². The dry season, spanning the months of November through March of the subsequent year, was characterized by a significant contraction of the water surface area, with a monthly maximum generally below 3,500 km², a minimum area below 2,000 km² (excluding March), and an average of approximately 2,500 km² (also excluding March).

The water area exhibits pronounced seasonal characteristics. It shows a progressively increasing trend from January to July, culminating in an annual peak in July. Subsequently, it follows a decreasing trend from July to December, reaching its annual trough. The peak area in July is approximately 1.5 times that of the trough in December. Both the average and maximum values follow a similar pattern of variation, reflecting the distinct seasonal nature of the lake basin. Although the minimum values show some fluctuations, they also reflect this seasonal change to a certain extent.

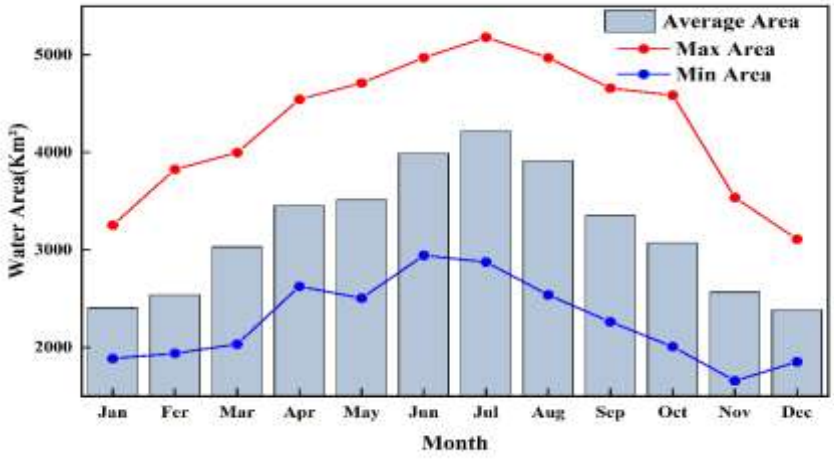

Figure 6: Monthly Water Surface Area (Max, Min, Avg) for Poyang Lake, 2016–2024.

The spatial dynamics of Poyang Lake's inundation (2016~2024), depicted in Figure 7, align with the statistical results, showing a pronounced seasonal rhythm of expansion and contraction. The southern and eastern portions of the main lake basin are where the most significant changes in the lake's surface area occur, with this process generally moving from the northeast to the southwest and featuring rapid expansion from March to May and rapid contraction from September to November.

The lake's narrow northern section, which serves as the outflow channel to the Yangtze River, is composed of river-like water bodies and exhibits greater stability compared to other areas. Similarly, low-lying lakes in the southernmost area, such as Junshan Lake which functions as a reservoir, maintain a more stable water cover in both the maximum and minimum monthly extents. Furthermore, each month exhibits a significant variation between its maximum and minimum extent, indicating the inter-annual instability of precipitation during the summer, as well as the potential occurrence of extreme drought events in some winters.

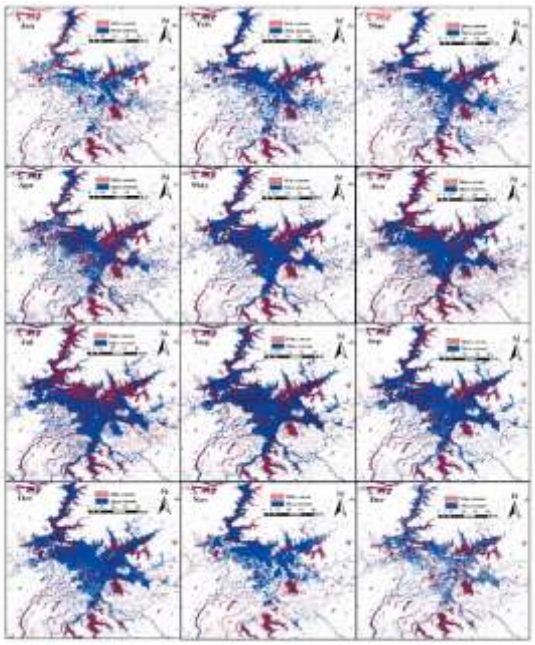

Figure 7: Maximum and Minimum Monthly Inundation Extent of Poyang Lake (2016–2024).

3.4. Analysis of Seasonal Variation in Poyang Lake (2016–2024)

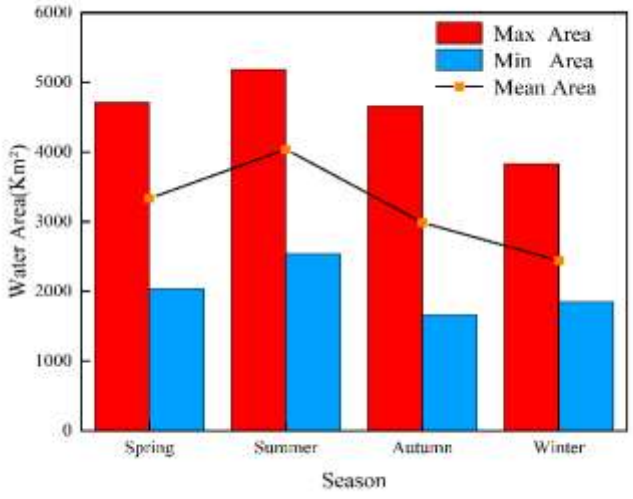

Figure 8: Seasonal Water Surface Area (Max, Min, Avg) for Poyang Lake, 2016–2024.

According to Figure 8, Poyang Lake's water area during spring and summer (March–August) is generally higher than in autumn and winter (September–February). Regarding the maximum inundation extent, the highest value is observed in summer (June–August) (5,179.38 km²), while the lowest occurs in winter (3,826.18 km²). Regarding the minimum water area, the largest extent was observed in summer (2537.97 km²) and the smallest in autumn (September–November) (1656.84 km²). For the average water surface area, summer is again the highest at 4,037.68 km², while winter is the lowest at 2,439.45 km².

A statistically insignificant increasing trend was observed for the water inundation extent in spring ($Z = 0.5842$, $p > 0.05$). In contrast, the water surface areas in all other seasons showed a downward trend. Specifically, winter ($Z = -2.3397$, $p < 0.05$) displayed a significant decreasing trend, while

summer (Z = -0.5140, p > 0.05) and autumn (Z = -1.0337, p > 0.05) showed non-significant decreasing trends (Figure 9).

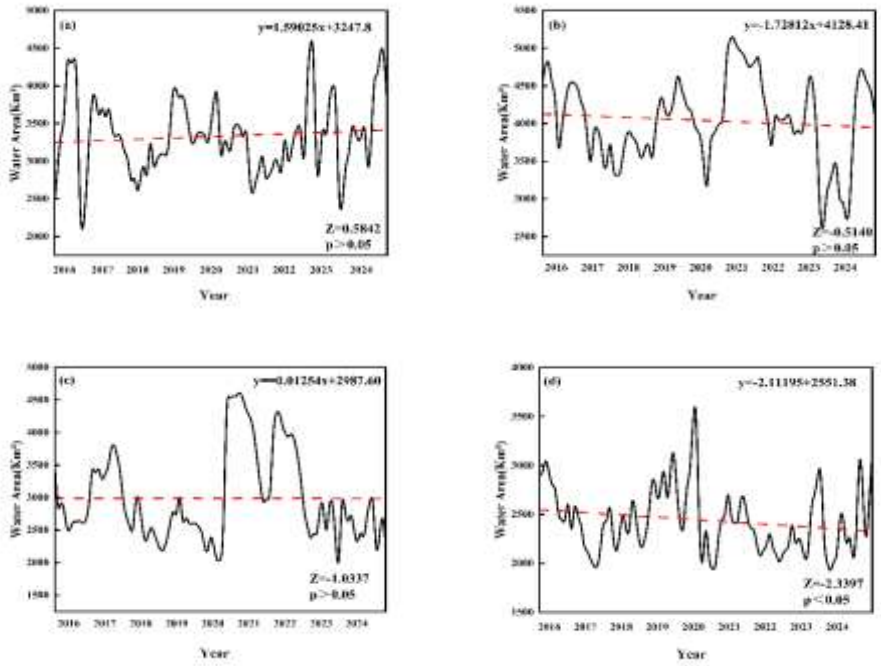

Figure 9: Seasonal area change trends of Poyang Lake Basin from 2016 to 2024 (a) spring, (b) summer, (c) autumn, (d) winter.

3.5. Analysis of Changes in Water Inundation Frequency

By calculating the water frequency, the water inundation extent of different water types for each year was obtained (Table 2). Among these, the seasonal water area demonstrated the most significant fluctuations, with its minimum proportion occurring in 2018 at 27.07% and its maximum in 2024 at 42.25%. From 2016 to 2018, it exhibited a gradual decreasing trend, from 2,097.34 km² to 1,600.82 km². This was followed by an increasing trend from 2018 to 2020, rising from 1,600.82 km² to 2,331.53 km². Subsequently, the area continuously decreased from 2020 to 2023, reaching 1,512.73 km², before showing a significant rebound in 2024.

Table 2: Areal Coverage and Percentage of Various Water Body Classes by Year (2016–2024)

	Temporary water/Km²	Seasonal water/Km²	Permanent water/Km²	Total area/Km²	Proportion of temporary water/%	Proportion of Seasonal water/%	Proportion of Permanent water/%
2016	1622.70	2097.34	2268.99	5989.03	27.09	37.89	35.02
2017	2088.56	1892.89	2144.41	6125.86	34.09	35.00	30.91
2018	2245.39	1600.82	2068.19	5914.39	37.96	34.97	27.07
2019	1958.94	2053.97	2107.39	6120.30	32.00	34.43	33.70
2020	1512.13	2321.53	2371.06	6204.72	24.37	38.21	37.42
2021	1766.02	2186.16	2088.07	6040.25	29.24	34.57	36.19
2022	1552.88	2180.62	1918.71	5652.20	27.47	33.94	38.59
2023	2026.01	1512.73	1858.02	5396.76	37.54	34.43	28.03
2024	1451.71	2538.76	2109.58	6010.05	24.15	33.60	42.25

A trend comparable to that of seasonal water was observed in the extent of permanent water bodies. This area reached its maximum of 2,371.06 km² in 2020 and its minimum of 1,858.02 km² in 2023.

For temporary water bodies, the minimum proportion was 24.15% in 2024, and the maximum was 37.96% in 2018. The area of these bodies gradually increased from 1622.70 km² to 2245.39 km² between 2016 and 2018, followed by a decreasing trend to1512.13 km² from 2018 to 2020. From 2020 to 2024, the changes were characterized by large-amplitude fluctuations.

A trend analysis of the three water body types from 2016–2024 revealed that only permanent water underwent a statistically significant change, showing a decline ($Z = -1.9809$, $p < 0.05$). In contrast, non-significant trends were observed for the other two types: a decrease in temporary water ($Z = -1.1468$, $p > 0.05$) and an increase in seasonal water ($Z = 0.7298$, $p > 0.05$).

As shown in Figure 10, the peripheries of the central lake and various low-lying areas, often comprising small ponds and farmland, are the primary locations for temporary water bodies. Seasonal water predominantly occupies the central part of the main lake basin, the banks along the northern channel, and southeastern parts of the lake. Accounting for a consistent 35% of the entire region, permanent water is primarily found in the central axis of the northern channel, the northeastern part of the lake, and low-lying southern basins such as Junshan Lake.

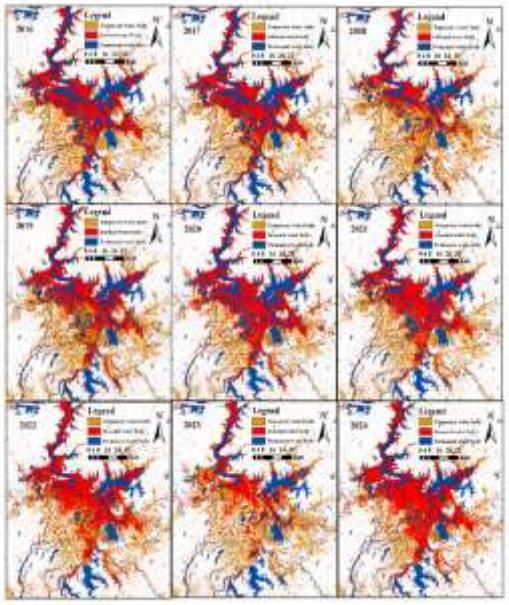

Figure 10: Spatial Distribution of Water Classifications. Red, yellow, and blue represent seasonal, temporary, and permanent water bodies respectively.

The proportion of temporary water bodies experienced large fluctuations around 2020 and during the 2022–2024 period. This corresponds with the flood events in Poyang Lake in 2020 and 2024, and the prolonged dry seasons due to droughts in 2022 and 2023, further demonstrating the significant impact of extreme events on water body dynamics.

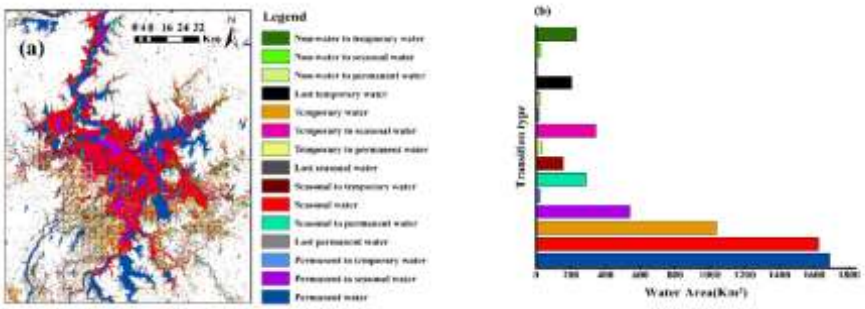

Figure 11: Conversions between Different Water Body Types (2016–2024). (a) Spatial distribution of the water type conversions. (b) Bar chart showing the area of each conversion class.

We analyzed the transformations among the three different water body types from 2016 to 2024. Figure 11 illustrates the spatial distribution of these conversions. An area of 4353.70 km² maintained a stable water body classification throughout the period, showing no conversion to other types. However, significant changes occurred among the different water body types. Permanent water coverage expanded by 329.41 km², with the majority of this gain (87.27%) resulting from the conversion of seasonal water, primarily on the sides of the channel zone at the entrance to the Yangtze River. Conversely, an area of 578.76 km² of permanent water was lost, of which 93.21% converted to seasonal water. This type of conversion was mainly concentrated in the lake's central region, its north-eastern part, and the northern channel zone at the entrance to the Yangtze River. The area of seasonal water bodies saw a gross increase of 911.02 km², with the vast majority (96.83%) originating from the conversion of permanent and temporary water. Conversely, an area of 469.67 km² of seasonal water was lost, of which 61.21% converted to permanent water and 33.52% converted to temporary water. The area of temporary water increased by 412.09 km², with most of this gain originating from the conversion of non-water areas. Simultaneously, it lost an area of 583.41 km²; apart from the portion that converted to seasonal water, the remaining majority converted back to non-water bodies.

The Poyang Lake basin gained 267.53 km² of new water bodies, with temporary water accounting for the vast majority of this increase (86.63%), which were converted from fish ponds and paddy fields. At the same time, the basin lost 246.81 km² of water bodies, the majority of which were temporary water, primarily distributed along the sides of river channels.

4. DISCUSSION

4.1. Correlation with Water Level Data

We correlated our extracted results with the DAHITI water level dataset and found a strong positive relationship (r=0.86), thereby confirming the reliability of our findings. Simultaneously, the resulting water level-area quadratic polynomial equation ($y = -37.26x^2 + 1388.35x - 8343.02$, $R^2 = 0.79$) (Figure 12) enables estimation of the inundation area from the water level and vice versa.

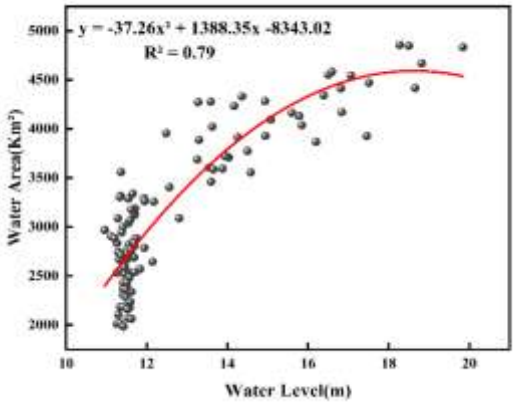

Figure 12: Water Level–Area Relationship.

4.2. Comparison with other datasets

Images from different periods across six randomly selected years were used to calculate the relative error between our extraction results and two other datasets (Table 3). The relative errors for both datasets were within 10%, indicating a strong agreement between our results and these two datasets. Furthermore, the trend of the lake's water inundation extent variation derived was compared with the

findings of other researchers, such as Wang et al. [23]. The variation patterns were found to be generally consistent.

Table 3: Comparison and relative error of water area extracted with other datasets

Time	Extracted water area/ Km²	JRC Monthly Water History/ Km²	Relative error/%	Global Surface Water Dynamics/ Km²	Relative error/%
August 2016	4469.95	4100.12	8.27%	4321.74	3.32%
September 2017	3404.43	3246.77	4.63%	3480.89	2.25%
February 2018	2312.51	2299.84	0.55%	2462.18	6.47%
January 2019	2768.22	2620.90	5.32%	2953.91	6.71%
October 2020	4283.30	4416.93	3.12%	4486.90	4.75%
September 2021	4163.14	3985.94	4.26%	4273.13	2.64%

4.3. Potential Factors

Anthropogenic activities are a likely driver of the observed fluctuations in Poyang Lake's water extent. Poyang Lake has a complex and intimate hydrological connection with the Yangtze River. This major hydro-engineering project on the Yangtze, the Three Gorges Dam, has enhanced human control over water resources; the dam's impoundment of water lowers the hydrological level of Poyang Lake, which in turn shrinks its inundation area. Anthropogenic activities such as sand dredging can lead to a decrease in the lakebed elevation at the outlet, which promotes a faster outflow of lake water, thereby reducing the lake's inundation extent.

Relevant data indicate that human activities such as lake reclamation and economic development have driven up the demand for water in the industrial, agricultural and domestic sectors, which in turn causes a contraction of the water surface of Poyang Lake and impairs its ecosystem functions. Lakes like Poyang and Dongting, which historically regulated Yangtze floods, have lost much of this capacity due to land reclamation projects. In response, the State Council of China has implemented a "Returning Farmland to Lake" policy, which aims to improve the capacity of Poyang Lake to both store and discharge floodwaters.

The findings of this research indicate that Poyang Lake's water surface area followed an upward trajectory between 2016 and 2024. In our analysis of conversions between different water body types, we found that the bulk of the new water area was sourced from existing fishponds and paddy fields. The expansion of the lake's area can be largely attributed to the promotion of the local "Returning Farmland to Lake" policy.

Temperature primarily affects water area by influencing evapotranspiration; therefore, the two factors of precipitation and evapotranspiration were selected for analysis. A Pearson correlation analysis revealed positive correlations for both factors at monthly and annual scales (Figure 13). Monthly precipitation and water area showed a correlation coefficient of 0.58, while for annual precipitation it was 0.90. The coefficient for monthly evapotranspiration and water area was 0.78, and for annual evapotranspiration, it was 0.59. Overall, annual precipitation and monthly evapotranspiration showed the highest correlations with water surface area.

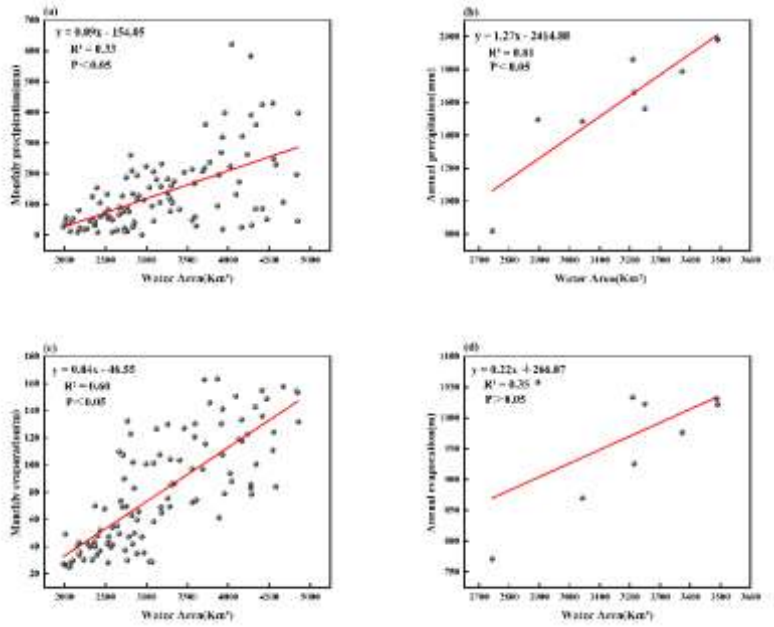

Figure 13: Relationship between Climatic Factors (Precipitation, Evaporation) and Water Surface Extent (a) Monthly precipitation, (b) Annual precipitation, (c) Monthly evaporation, (d) Annual evaporation.

4.4. Restrictions and Limitations

Regarding the data source, this study exclusively used data from the Sentinel series of satellites. The Sentinel constellation offers advantages such as higher spatial resolution and a short revisit period, which facilitates the high-frequency extraction of the lake's area. Furthermore, Sentinel-1 imagery is unaffected by weather conditions. However, due to the relatively recent launch of the Sentinel satellites, this research was constrained to analyzing water body changes from 2016 to 2024.

In the analysis of driving factors, this study is not sufficiently comprehensive. This limitation stems from two primary issues: first, the considerable difficulty in acquiring local hydrological data, and second, the complex nature of the impacts exerted by climatic and anthropogenic activities on the water body.

Future research directions include extending the analysis over a longer time-series by integrating multiple data sources to better explore long-term dynamics. Additionally, future studies should incorporate more of these influencing factors and should conduct not only qualitative but also quantitative analyses.

5. CONCLUSIONS

Through the dynamic observation of Poyang Lake's water bodies over the 2016–2024 period and the analysis of their spatiotemporal dynamic characteristics, the following conclusions can be drawn:

(1) The results indicate that the extraction algorithm used in this study, which combines Sentinel-1/2 data, performs well in the Poyang Lake basin. The overall accuracies for the two validation images reached 98.9% and 96.43%, with Kappa coefficients of 97.87% and 91.87%, respectively. This proves that the algorithm can be reliably used for fine-scale analysis of the lake's hydrological dynamics.

(2) The Poyang Lake basin underwent significant fluctuations in its water body area from 2016 to 2024. The maximum inundation area occurred in 2020, reaching 5,179.37 km², while the minimum inundation area was observed in 2022 at 3,196.04 km².

(3) The data analysis shows that the lake's inundation area exhibits a strong sea-sonal pattern of rise and fall. Typically, June and July represent the months of greatest water extent, whereas November and December have the smallest. The water surface area is generally higher in spring and summer. Regarding seasonal trends, the water area in spring shows an upward trend, while the remaining seasons all exhibit a downward trend.

(4) In the analysis of water frequency, permanent and temporary water bodies are decreasing, while seasonal ones are increasing. Spatially, temporary water is primarily concentrated at the margins of the central lake region. Seasonal water is predominantly found in the lake's central region. The primary locations for permanent water are the center of the northern channel zone and low-lying southern lakes such as Junshan Lake. The conversion between water body types was dominated by the transformation of temporary and permanent water into seasonal water.

ACKNOWLEDGEMENTS

Thanks to H.J. for providing the lab environment.

REFERENCES

[1] Che, X., Feng, M., Sun, Q., Sexton, J. O., Channan, S., & Liu, J. (2021). The decrease in lake numbers and areas in central asia investigated using a landsat-derived water dataset. Remote Sensing, 13(5), 1032.

[2] Maavara, T., Chen, Q., Van Meter, K., Brown, L. E., Zhang, J., Ni, J., & Zarfl, C. (2020). River dam impacts on biogeochemical cycling. Nature Reviews Earth & Environment, 1(2), 103-116.

[3] Cui, X., Guo, X., Wang, Y., Wang, X., Zhu, W., Shi, J., ... & Gao, X. (2019). Application of remote sensing to water environmental processes under a changing climate. Journal of Hydrology, 574, 892-902.

[4] Pekel, J. F., Cottam, A., Gorelick, N., & Belward, A. S. (2016). High-resolution mapping of global surface water and its long-term changes. Nature, 540(7633), 418-422.

[5] Huang, C., Chen, Y., Zhang, S., & Wu, J. (2018). Detecting, extracting, and monitoring surface water from space using optical sensors: A review. Reviews of Geophysics, 56(2), 333-360.

[6] Chung, M. G., Frank, K. A., Pokhrel, Y., Dietz, T., & Liu, J. (2021). Natural infrastructure in sustaining global urban freshwater ecosystem services. Nature Sustainability, 4(12), 1068-1075.

[7] Pokhrel, Y., Felfelani, F., Satoh, Y., Boulange, J., Burek, P., Gädeke, A., ... & Wada, Y. (2021). Global terrestrial water storage and drought severity under climate change. Nature Climate Change, 11(3), 226-233.

[8] Cao, H., Han, L., Liu, Z., & Li, L. (2021). Monitoring and driving force analysis of spatial and temporal change of water area of Hongjiannao Lake from 1973 to 2019. Ecological Informatics, 61, 101230.

[9] Li, L., Vrieling, A., Skidmore, A., Wang, T., & Turak, E. (2018). Monitoring the dynamics of surface water fraction from MODIS time series in a Mediterranean environment. International journal of applied earth observation and geoinformation, 66, 135-145.

[10] Yao, F., Wang, J., Wang, C., & Crétaux, J. F. (2019). Constructing long-term high-frequency time series of global lake and reservoir areas using Landsat imagery. Remote Sensing of Environment, 232, 111210.

[11] Schwatke, C., Scherer, D., & Dettmering, D. (2019). Automated extraction of consistent time-variable water surfaces of lakes and reservoirs based on Landsat and Sentinel-2. Remote Sensing, 11(9), 1010.

[12] Li, X., Ling, F., Foody, G. M., Boyd, D. S., Jiang, L., Zhang, Y., ... & Du, Y. (2021). Monitoring high spatiotemporal water dynamics by fusing MODIS, Landsat, water occurrence data and DEM. Remote Sensing of Environment, 265, 112680.

[13] Liu, Q., Huang, C., Shi, Z., & Zhang, S. (2020). Probabilistic river water mapping from Landsat-8 using the support vector machine method. Remote Sensing, 12(9), 1374.

[14] Tulbure, M. G., Broich, M., Stehman, S. V., & Kommareddy, A. (2016). Surface water extent dynamics from three decades of seasonally continuous Landsat time series at subcontinental scale in a semi-arid region. Remote Sensing of Environment, 178, 142-157.

[15] Zou, Z., Xiao, X., Dong, J., Qin, Y., Doughty, R. B., Menarguez, M. A., ... & Wang, J. (2018). Divergent trends of open-surface water body area in the contiguous United States from 1984 to 2016. Proceedings of the National Academy of Sciences, 115(15), 3810-3815.

[16] Xing, N., Gan, F., Yan, B., Bai, J., Guo, Y., Zhuo, Y., & Li, R. (2024). Dynamic Monitoring and Change Analysis of Lake Area on the Inner-Mongolian Plateau over the Past 22 Years. Remote Sensing, 16(12), 2210.

[17] Deng, Y., Jiang, W., Tang, Z., Ling, Z., & Wu, Z. (2019). Long-term changes of open-surface water bodies in the Yangtze River basin based on the Google Earth Engine cloud platform. Remote Sensing, 11(19), 2213.

[18] Xing, W., Guo, B., Sheng, Y., Yang, X., Ji, M., & Xu, Y. (2022). Tracing surface water change from 1990 to 2020 in China's Shandong Province using Landsat series images. Ecological Indicators, 140, 108993.

[19] Wang, C., Jiang, W., Deng, Y., Ling, Z., & Deng, Y. (2021). Long time series water extent analysis for SDG 6.6. 1 based on the GEE platform: A case study of Dongting Lake. IEEE Journal of Selected Topics in Applied Earth Observations and Remote Sensing, 15, 490-503.

[20] Yang, X., Qin, Q., Yésou, H., Ledauphin, T., Koehl, M., Grussenmeyer, P., & Zhu, Z. (2020). Monthly estimation of the surface water extent in France at a 10-m resolution using Sentinel-2 data. Remote Sensing of Environment, 244, 111803.

[21] Zeng, L., Schmitt, M., Li, L., & Zhu, X. X. (2017). Analysing changes of the Poyang Lake water area using Sentinel-1 synthetic aperture radar imagery. International Journal of Remote Sensing, 38(23), 7041-7069.

[22] Markert, K. N., Markert, A. M., Mayer, T., Nauman, C., Haag, A., Poortinga, A., ... & Saah, D. (2020). Comparing sentinel-1 surface water mapping algorithms and radiometric terrain correction processing in southeast asia utilizing google earth engine. Remote Sensing, 12(15), 2469.

[23] Wang, Z., Xie, F., Ling, F., & Du, Y. (2022). Monitoring surface water inundation of Poyang Lake and Dongting Lake in China using Sentinel-1 SAR images. Remote Sensing, 14(14), 3473.

[24] Guo, S., Chen, Y., Zhang, P., Zhang, W., Tang, P., Fang, H., ... & Du, P. (2024). Estimates and dynamics of surface water extent in the Yangtze Plain from Sentinel-1&2 observations. International Journal of Applied Earth Observation and Geoinformation, 134, 104155.

[25] Schwatke, C., Dettmering, D., Bosch, W., & Seitz, F. (2015). DAHITI–an innovative approach for estimating water level time series over inland waters using multi-mission satellite altimetry. Hydrology and Earth System Sciences, 19(10), 4345-4364.

[26] Pickens, A. H., Hansen, M. C., Hancher, M., Stehman, S. V., Tyukavina, A., Potapov, P., ... & Sherani, Z. (2020). Mapping and sampling to characterize global inland water dynamics from 1999 to 2018 with full Landsat time-series. Remote Sensing of Environment, 243, 111792.

[27] Farr, T. G., Rosen, P. A., Caro, E., Crippen, R., Duren, R., Hensley, S., ... & Alsdorf, D. (2007). The shuttle radar topography mission. Reviews of geophysics, 45(2).

[28] Yamazaki, D., Ikeshima, D., Sosa, J., Bates, P. D., Allen, G. H., & Pavelsky, T. M. (2019). MERIT Hydro: A high-resolution global hydrography map based on latest topography dataset. Water Resources Research, 55(6), 5053-5073.

[29] Yuchen, L. I. U., & Yongnian, G. A. O. (2022). Surface water extraction in Yangtze River Basin based on sentinel time series image. National Remote Sensing Bulletin, 26(2), 358-372.

[30] Modification of normalised difference water index (NDWI) to enhance open water features in remotely sensed imagery

[31] Feyisa, G. L., Meilby, H., Fensholt, R., & Proud, S. R. (2014). Automated Water Extraction Index: A new technique for surface water mapping using Landsat imagery. Remote sensing of environment, 140, 23-35.

[32] Tucker, C. J. (1979). Red and photographic infrared linear combinations for monitoring vegetation. Remote sensing of Environment, 8(2), 127-150.

[33] Huete, A., Didan, K., Miura, T., Rodriguez, E. P., Gao, X., & Ferreira, L. G. (2002). Overview of the radiometric and biophysical performance of the MODIS vegetation indices. Remote sensing of environment, 83(1-2), 195-213.

[34] Liu, Y., Lai, L., & Gao, Y. (2023). Mapping 10 m monthly surface water dynamics in the yangtze river basin from 2017 to 2020 using a robust atmc algorithm. Journal of Hydrology, 626, 130327.